ACS central science

http://pubs.acs.org/journal/acscii

Research Article

Fabrication of Photoresponsive Crystalline Artificial Muscles Based on PEGylated Covalent Organic Framework Membranes

Xiuxiu Guo, Tianhui Mao, Zhifang Wang, Peng Cheng, Yao Chen, Shengqian Ma, and Zhenjie Zhang*

Cite This: https://dx.doi.org/10.1021/acscentsci.0c00260

Read Online

ACCESS | Metrics & More | Article Recommendations | Supporting Information

ABSTRACT: Seeking new photoresponsive materials with high energy conversion efficiency, good mechanical properties, as well as well-defined photoactuation mechanisms is of paramount significance. To address these challenges, we first introduced crystalline covalent organic frameworks (COFs) into the photoactuator field and created a facile fabrication strategy to directly install photoresponsive functional groups (i.e., acylhydrazone) on the skeletons of COFs. Herein, an approach to use polyethylene glycol (PEG) cross-linked dimers as the building blocks of the **COF-42** platform was developed and afforded a series of uniform and freestanding membranes (**PEG-COF-42**) with outstanding mechanical properties (e.g., high flexibility and mechanical strength). Notably, these membranes possessed a fast mechanical response (e.g., bending) to UV light and good reversibility upon blue light or heating. After an in-depth investigation of the photoactuation mechanism via various techniques, we proposed a mechanism for the photoresponsive performance of **PEG-COF-42**: configurational change of acylhydrazone (i.e., E ↔ Z isomerization) accompanied by an excited-state intramolecular proton transfer (ESIPT) process intramolecularly transferring hydrogens from hydrogen donors (N—H) to hydrogen acceptors (oxygen in PEG). Moreover, attributed to the PEG moieties, **PEG-COF-42** also demonstrated a vapor-responsive performance. This study not only broadens the application scopes of COFs but also provides new opportunities for the construction of multi-stimuli-responsive materials.

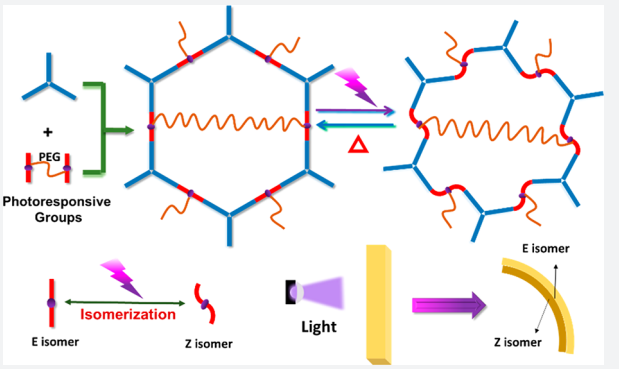

INTRODUCTION

Smart materials that can convert various forms of stimuli (e.g., heat, light, electric field, magnetic field, pH, moisture) to mechanical motions are currently attracting intense attention.[1−4] Among all stimuli, light possesses intrinsic advantages such as wireless control, abundant light sources with variable wavelengths, cost-effectiveness, cleanliness, and safety.[5] Photomechanical smart materials have demonstrated great potential for applications as diverse as information storage, sensors, actuators, artificial muscles, self-healing materials, and so forth.[6−8] Until now, photomechanical smart materials have been mostly concentrated on carbon-based materials[9] and polymeric materials including organic polymers,[10] liquid-crystalline elastomers,[11] hydrogels,[12] and biopolymers.[13] However, these materials usually possess no or low crystallinity that unavoidably lead to low intrinsic energy conversion efficiencies, impeding their application scopes. In other words, the arrangement of photoresponsive chromophores (e.g., azobenzene,[14−16] anthracenes,[17−20] diarylethenes[21]) in material structures is not or partially in an order that often leads to low coupling efficiency between light and mechanical energy.[22] Thus, developing new photoresponsive materials with high energy conversion efficiency, well-defined photoactuation mechanisms, and robust mechanical properties is of high importance and in urgent demand.

Recently, molecular crystals have demonstrated great promise as smart materials due to their advantages such as well-defined crystal structures, faster response time, and shorter recovery time.[23] The energy transfer between stimuli and active groups is more efficient in crystalline structures with less energy dissipation. However, molecular crystals possess intrinsic disadvantages such as brittleness, low processability, and small size that seriously hinder their practical applications such as performing useful work (motion) or fabricating large devices. Thanks to the pioneering work of Yaghi in 2005,[24] covalent organic frameworks (COFs) have emerged as a new generation of crystalline polymeric materials that combine the benefits of molecular crystals and organic polymers, such as high crystallinity,[25] precisely determined structures,[26] high porosity,[27] tunable pore size,[28] good processability,[29−31] customizable functionality, and so on.[32−40] Ascribed to these advantages, COFs can serve as an ideal class of materials for

Received: March 4, 2020

photomechanical applications. Nevertheless, to the best of our knowledge, there has been no report using COFs as photomechanical smart materials yet.

In order to prepare photomechanical COFs, a facile fabrication strategy is to directly install photoresponsive functional groups (e.g., azobenzene,[41] hydrazone[42]) on COFs' skeletons (Scheme 1). The hydrazone functional

Scheme 1. Schematic Illustration of the Construction Approach of Photomechanical COFs

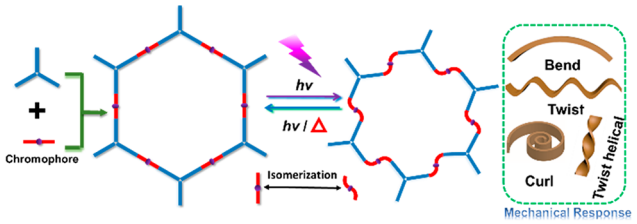

group, especially acylhydrazone, is perfectly suited to realize this strategy due to the following concerns.[42] (i) A light stimulus can highly efficiently activate the E ↔ Z isomerization (i.e., configurational switching) of acylhydrazones, accompanied by a reversible change of materials' properties such as volume, shape, and fluorescence.[43−45] (ii) There are some classic COFs (e.g., **COF-42**, **COF-43**)[46] based on acylhydrazone linkages that exhibit superior advantages such as rapid and scalable synthesis,[47] high stability, and facile membrane formation.[48] In this study, we applied **COF-42** as a platform and engineered **COF-42** with polyethylene glycol (PEG) bridging linkers that afforded a series of uniform, freestanding, and defect-free membranes. The formed **PEG-COF-42** membranes exhibited an excellent mechanical property (high flexibility and good mechanical strength) and a reversible photoresponsive and vapor-responsive performance. This study paves a new avenue to prepare multi-stimuli-responsive materials based on COFs.

RESULTS AND DISCUSSION

Synthesis and Characterization of PEG-COF-42 Membranes. Forming membranes with good mechanical properties (e.g., high flexibility and mechanical strength) is highly desirable for mechanically responsive smart materials since materials need to hold the internal or external mechanical forces without fracture and destruction. According to the literature, the **COF-42** membrane possessed a very weak mechanical property (e.g., easily broke upon mechanical force) (Figure 1 and Figure S1).[49] To improve the mechanical properties of **COF-42**, recently, our group has developed a "polyCOF" strategy via introducing PEGylated chain polymers as the building blocks of **COF-42**.[49] It was found that introducing chain polymers into COF structures not only can significantly improve the membrane formation ability and quality, and greatly enhance the mechanical performance, but also can endow new properties to COFs, such as a vapor-responsive performance. However, this strategy still exhibited some drawbacks: (i) a synthesis challenge of polymeric building blocks; (ii) relatively high polydispersity index (PDI) of polymers; and (iii) small monomers required to serve as co-building blocks to obtain a membrane with high crystallinity.

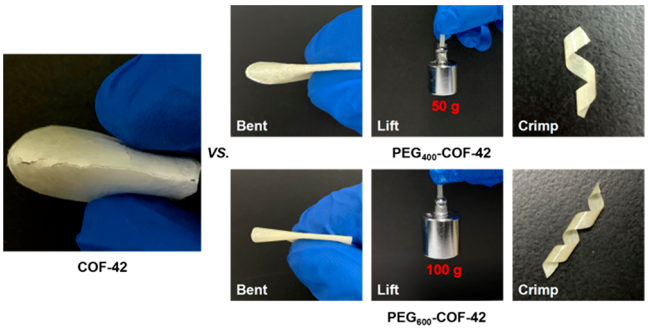

Figure 1. Comparison of the mechanical performance of **PEG-COF-42** (intact upon bending, lifting, and crimping operations) vs **COF-42** (fracture upon bending) membranes.

To address these issues, in this contribution, we developed a more feasible and simpler approach using 2,5-diethoxyterephthalohydrazide (DTH) dimer with PEG bridging linkers (DTH-dimer-*x*, *x* = molecular weight of PEG) as the monomer of **COF-42**. Uniform and freestanding **PEG-COF-42** membranes were harvested via interfacial polycondensation of 1,3,5-benzenetricarboxaldehyde (TB) with DTH-dimer-*x* at room temperature (Figure 2a and Figure S1). Further investigation

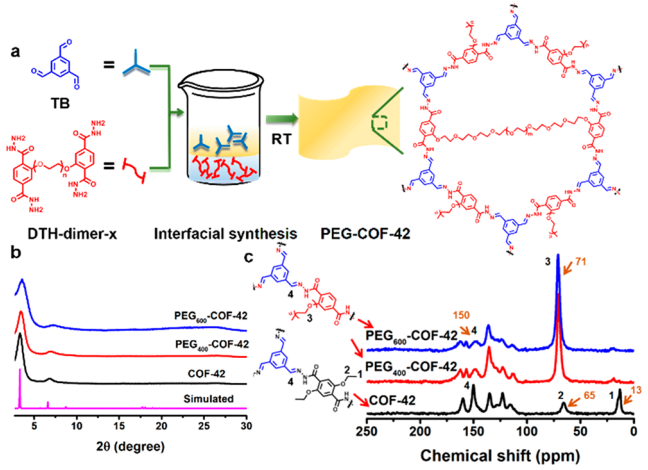

Figure 2. (a) Illustration of the approach to fabricate **PEG-COF-42** membrane using interfacial synthesis. PXRD patterns (b) and solid-state ^{13}C NMR (c) of **COF-42** and **PEG-COF-42**.

revealed that the appropriate length of PEG linkers is crucial for the formation of crystalline membranes. Powder X-ray diffraction (PXRD) data showed that **PEG$_x$-COF-42** (x = 400 or 600) membranes possessed high crystallinity with the characteristic peak at 3.4°, 7.0°, and 26.9° as pristine **COF-42** (Figure 2b).[46] By contrast, PEG linkers with a molecule weight of 150 or 800 g/mol afforded amorphous materials due to the mismatching of PEG size and pore space (Figures S2 and S3). These results indicate that PEG linkers with the appropriate length would form interlayer or intralayer cross-linking in the **COF-42** skeleton (Figure S3) without affecting the pristine crystallinity of COFs. We also found that the porosity and pore size of **PEG-COF-42** significantly decreased due to the blockage of COFs' channels by PEG moieties, and the longer PEG linker induced a lower porosity (pore volume and Langmuir surface area of 0.32 cm^3/g and 782 m^2/g, 0.15 cm^3/g and 101 m^2/g, and 0.01 cm^3/g and 22 m^2/g for **COF-42**,

https://dx.doi.org/10.1021/acscentsci.0c00260
ACS Cent. Sci. XXXX, XXX, XXX−XXX

PEG_{400}-COF-42, and **PEG_{600}-COF-42**, respectively) (Figure S4).

Various solid-state characterization techniques were then applied to characterize **PEG-COF-42** membranes. Fourier transform infrared (FT-IR) spectra exhibited new vibration bands at 1619 and 1221 cm^{-1} attributed to the formation of the C═N bonds. Meanwhile, the increase of characteristic peaks of C—H (2870 cm^{-1}) and C—O (1100 cm^{-1}) indicated the existence of PEG chains (Figure S4c).[50] The ^{13}C CP-MAS NMR result further validated the formation of **PEG_{400}-COF-42** and **PEG_{600}-COF-42**. The characteristic signal at 150 ppm is ascribed to the chemical shift of the C═N bonds for **PEG-COF-42**. With the introduction of PEG, the peaks of ethyl groups (13 and 65 ppm) in **COF-42** disappeared, and a new peak (71 ppm) assigned to carbons in PEG chains was observed in **PEG-COF-42** (Figure 2c).

The quality of **PEG-COF-42** membrane is evaluated using scanning electron microscopy (SEM) and stress−strain tests. SEM images showed that **PEG-COF-42** presented as homogeneous, cohesive, and freestanding membrane structures (Figure 3 and Figure S5). Cross-sectional SEM images further

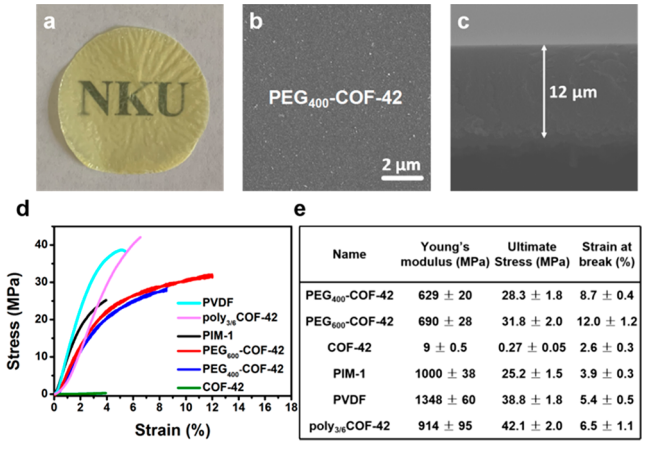

e

Name	Young's modulus (MPa)	Ultimate Stress (MPa)	Strain at break (%)
PEG_{400}-COF-42	629 ± 20	28.3 ± 1.8	8.7 ± 0.4
PEG_{600}-COF-42	690 ± 28	31.8 ± 2.0	12.0 ± 1.2
COF-42	9 ± 0.5	0.27 ± 0.05	2.6 ± 0.3
PIM-1	1000 ± 38	25.2 ± 1.5	3.9 ± 0.3
PVDF	1348 ± 60	38.8 ± 1.8	5.4 ± 0.5
$poly_{3/6}$COF-42	914 ± 95	42.1 ± 2.0	6.5 ± 1.1

Figure 3. (a) Photograph of transparent **PEG_{400}-COF-42** membrane. (b) Top view and (c) cross-section SEM images of **PEG_{400}-COF-42**. (d) Stress−strain curves for **PEG-COF-42** vs **COF-42**, **PIM-1**, PVDF, and **$poly_{3/6}$COF-42** membranes. (e) Mechanical analysis of the stress−strain curves.

revealed a uniform, compact particle packing nature (thickness of **PEG_{400}-COF-42**, 12 μm; **PEG_{600}-COF-42**, 14 μm) (Figure 3c and Figure S5). In order to protrude the advantages of **PEG-COF-42**, we also prepared a **COF-42** membrane via the same procedure (i.e., interfacial polycondensation of TB and DTH) as **PEG-COF-42**. SEM images revealed that the **COF-42** membrane exhibited a rough surface with loosely packed particles (Figure S5). Additionally, stress−strain experiments revealed that the toughness and Young's modulus of **PEG_{400}-COF-42** and **PEG_{600}-COF-42** membranes were greatly improved, compared with the pristine **COF-42** membranes (Figure 3d and Table S1). For instance, **PEG_{600}-COF-42** achieved the highest elongation of 12%, almost 5 times as much as the **COF-42** membrane (2.6%) and 2 times better than our previously reported **$poly_{3/6}$COF-42** membrane (6.5%). The elongations at break of **PEG_{400}-COF-42** and **PEG_{600}-COF-42** are even higher than some commercial or classic polymeric membranes (e.g., **PIM-1**, PVDF, **$poly_{3/6}$COF-42**) (Figure 3e). Furthermore, the **PEG-COF-42** membrane can proceed repeatedly with deformations (e.g., bent, twisted, or stretched) without damage (Figure 1). Notably, **PEG_{600}-COF-42** membranes possessed the highest toughness to lift a steel object of 100 g. Overall, attributed to the cross-linking effect of PEG bridging linkers, the mechanical performance of **PEG-COF-42** membranes was much better than the pristine **COF-42** membranes.

Evaluation of the Mechanically Responsive Performance of PEG-COF-42. The E ↔ Z isomerization of the acylhydrazone group triggered by light is always accompanied by a reversible change of materials' properties such as volume and shape. Noteworthily, we found that **PEG_{400}-COF-42** and **PEG_{600}-COF-42** membranes were photoresponsive to UV light with reversible bending behaviors (Figure S6). Herein, **PEG_{400}-COF-42** membrane was selected as a representative to demonstrate the stimuli-responsive behavior. UV/vis spectroscopy unveiled absorption bands of λ_{max} = 375 nm for **PEG_{400}-COF-42** in the UV region (Figure S7). Thus, we selected UV light with λ_{irr} = 370 nm (288 mW/cm^2) to trigger the E ↔ Z isomerization of acylhydrazone groups in **PEG_{400}-COF-42**. **PEG_{400}-COF-42** membranes were cut into a strip (12 mm × 3 mm) fixed on a glass fiber and irradiated with unilateral UV light in the vertical direction. We used the displacement (D) and bending angle (θ) to evaluate the degree of the mechanical response process (Figure 4a). It was found that the **PEG_{400}-**

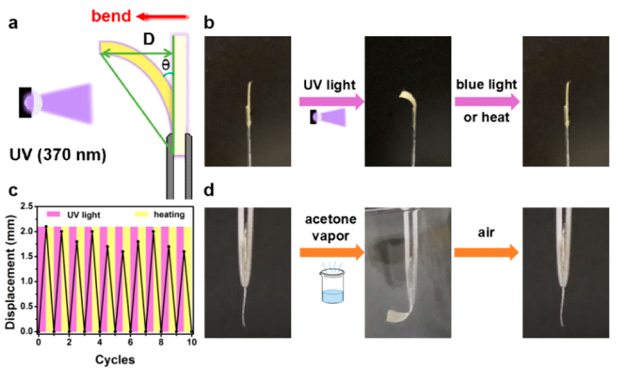

Figure 4. (a) Schematic illustration of the defined displacement (D) and bending angle (θ) in the mechanically responsive process. (b) Photoresponsive bending behavior of the **PEG_{400}-COF-42** membrane. (c) Plot of the reversible cycles of **PEG_{400}-COF-42** via UV irradiation and heating. (d) Vapor-responsive bending behavior of the **PEG_{400}-COF-42** membrane.

COF-42 strip gradually bent toward the light to reach a maximum bending angle of θ = 30° in as short as 20 s. This photoresponsive bending performance is better than some state-of-the-art materials (e.g., **trans-1**).[51] Notably, through irradiation with 440 nm blue light (288 mW/cm^2) from the same direction for 3 min at room temperature or thermal treatment at 100 °C for 1 min, membranes can bend back to the initial position (Figure 4b). This reversible bending performance can be repeated for many cycles with alternating UV light and thermal treatment (Figure 4c). As mentioned in the literature,[42,43] the E state of acylhydrazone-based compounds is thermal dynamically more stable than the Z state, hence leading to the E → Z transformation upon heat. Moreover, the behavior of bending toward light indicates that the side of **PEG-COF-42** membrane close to light conducted a volume shrinkage during the light irradiation.

https://dx.doi.org/10.1021/acscentsci.0c00260
ACS Cent. Sci. XXXX, XXX, XXX−XXX

PEG-COF-42 membranes also can inherit the property of PEG-based building blocks.[49] When exposed to the acetone vapor, **PEG-COF-42** membranes showed a fast bending response in 2 s to achieve a bending angle of θ = 40° and can rapidly recover back to the initial position once exposed to air (Figure 4d). Notably, this reversible bending process can undergo >20 cycles without fatigue (Figures S8 and S9). As reported in our previous work, pure **COF-42** membrane did not exhibit vapor-responsive behavior due to the lack of PEG moieties, while the pure PEG membrane exhibited a reversible vapor-responsive performance. Thus, we can conclude that the vapor-responsive property of **PEG-COF-42** membranes originated from PEG moieties which can reversibly change their conformation upon a vapor stimulus. Taking advantage of the vapor-responsive and photoresponsive behaviors of **PEG-COF-42** membranes, fabrication of multi-stimuli-responsive actuators to perform complicated motions is ongoing in our lab.

Investigating the Mechanism of the Photomechanical Response of PEG-COF-42. Various solid-state characterization techniques were applied to unveil the mechanism behind the photomechanical performance of **PEG-COF-42**. Herein, we further chose **PEG$_{400}$-COF-42** as a representative. **PEG$_{400}$-COF-42** before light irradiation exhibits the E isomer (named as **PEG$_{400}$-COF-42(E)**).[43] After irradiation with 370 nm UV light for 12 h, a broader UV spectrum band centered around λ_{max} = 400 nm appeared (Figure 5a), indicating the isomerization to **PEG$_{400}$-COF-42(Z)**. SEM and ^{13}C NMR spectra before and after light irradiation showed no obvious changes (Figures S10 and S11), indicative of no bond breaking occurring during the UV light irradiation. The PXRD pattern after UV irradiation showed the same pattern as pristine **PEG$_{400}$-COF-42**, but with a decrease of peak intensity (Figure S12). It is possibly due to the partial loss of coherence of molecular building blocks in COFs. Upon irradiation to light, local disorientation is likely to take place, which makes the molecular building blocks deviate from their original lattice positions, hence leading to local incoherence, while their overall positions are maintained to afford almost identical peak positions but with lower intensity.

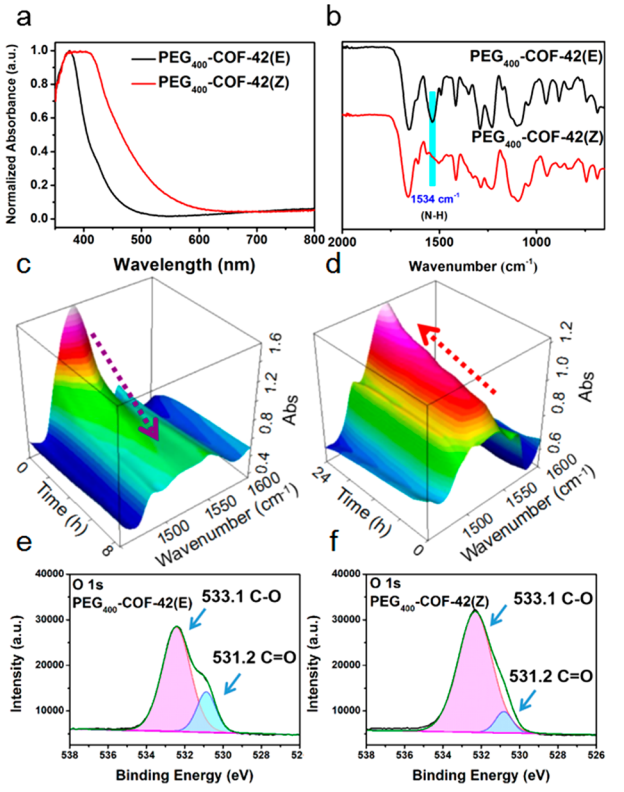

Figure 5. (a) Solid-state UV−vis absorption spectra of **PEG$_{400}$-COF-42** before and after UV irradiation. (b) FT-IR spectra of **PEG$_{400}$-COF-42** before and after UV irradiation. (c) In situ FT-IR spectra of the **PEG$_{400}$-COF-42** membrane under UV irradiation with different times. (d) In situ FT-IR spectra of the **PEG$_{400}$-COF-42** membrane at 100 °C. XPS O 1s signals for **PEG$_{400}$-COF-42** before (e) and after (f) UV irradiation.

The fluorescent spectrum of **PEG$_{400}$-COF-42(E)** possessed a characteristic emission peak at 470 nm upon excitation at 365 nm (Figure S13). According to the literature, the fluorescent property of **PEG$_{400}$-COF-42(E)** can be attributed to the excited-state intramolecular proton transfer (ESIPT) mechanism which is a process of intramolecularly transferring protons from donor groups (i.e., N—H) to proton acceptor groups (i.e., oxygen− in PEG) under light irradiation.[52,53] After UV irradiation, the intensity of the characteristic emission peak decreased in **PEG$_{400}$-COF-42(Z)**, possibly due to the configurational change (i.e., E ↔ Z isomerization) of acylhydrazone that hindered the ESIPT process.[52] As reported by Lehn,[54] Aprahamian,[42] and Hecht,[43] acylhydrazone switches triggered by stimuli conducted isomerization through either an out-of-plane rotation of the double bond or in-plane nitrogen inversion of C═N. In **PEG-COF-42**, due to the stacking of 2-dimentional (2D) COF layers, out-of-plane rotation is forbidden. Thus, the isomerization is possibly through an in-plane nitrogen inversion of C═N. Moreover, the Z isomer can be stabilized through noncovalent interactions in **PEG-COF-42**, such as $\pi\cdots\pi$ interaction and intralayer/interlayer hydrogen bonding.[47]

In situ FT-IR, Raman and X-ray photoelectron spectroscopy (XPS) were further used to study the photoreactions that occurred during the light irradiation. As shown in the FT-IR spectra (Figure 5c), the intensity of the characteristic peak at 1540 cm^{-1} ascribed to the bending vibration of the N—H group in acylhydrazone gradually decreased as irradiation time extended. We also observed that the decreasing rate of peak intensity is faster in the initial stage and then gradually slowed down (Figure 5c and Figure S14). The Raman spectra clearly showed the disappearance of the peak at 1560 cm^{-1}, which is also ascribed to the change of the N—H group (Figure S15). Interestingly, when the **PEG$_{400}$-COF-42(Z)** membrane obtained after UV irradiation was placed in a 100 °C oven, FT-IR spectra revealed that the bending vibration at 1540 cm^{-1} gradually increased, indicative of the reversible nature of the proton transfer process (Figure 5d and Figure S16). The XPS O 1s signals of **PEG$_{400}$-COF-42** before and after UV irradiation are compared in Figure 5e,f. It was found that the relative intensity of C═O (531.2 eV) compared with C—O (533.1 eV) dramatically decreased after UV irradiation.[45] The C 1s signals of **PEG$_{400}$-COF-42** did not show significant change before and after UV irradiation (Figure S17). These results indicate that a tautomerism (e.g., enolate-keto) exists in the ESIPT process (Figure 6a).

According to the ESIPT mechanism, the photoexcited molecule can tautomerize through proton transfer. This agrees well with the result of XPS, FT-IR, and Raman spectra data. As illustrated in Figure 6a, the N—H group in the skeleton of

https://dx.doi.org/10.1021/acscentsci.0c00260
ACS Cent. Sci. XXXX, XXX, XXX−XXX

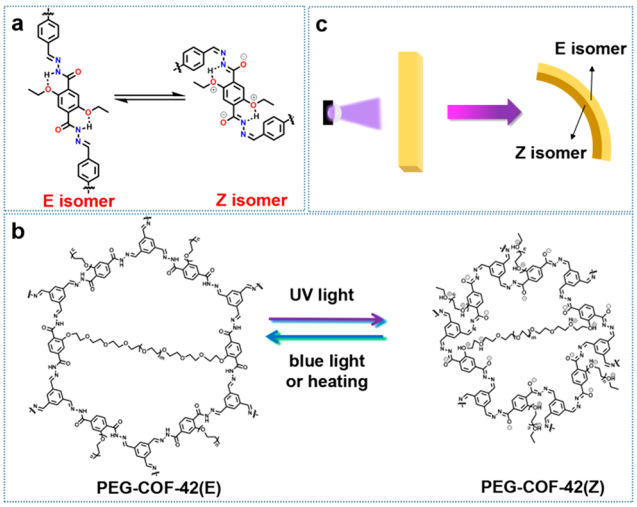

Figure 6. (a) Illustration of the possible mechanism of the E ↔ Z isomerization. (b) Mechanism to explain the bending toward light behavior of **PEG-COF-42** membranes. (c) Proposed structure changes of **PEG-COF-42** under UV irradiation.

PEG-COF-42(E) can form intramolecular hydrogen bonding with oxygen from alkoxy moieties in a six-membered ring fashion. After the photoreaction, the proton acceptor (i.e., oxygens in PEG) can capture a hydrogen from the adjacent N—H group to form a six-membered ring with adjacent nitrogen. In order to prove the crucial role of alkoxy moieties to the proton transferring reaction, we further prepared **COF-42** and its analogues (Figures S18−S20) as a comparison. **TB-Th COF** was synthesized via the reaction of TB and terephthalohydrazide (TPHD). Due to the absence of the alkoxy group, the ESIPT process cannot occur in **TB-Th COF**, proven by FT-IR data with no change before and after UV irradiation for 12 h (Figure S21). **DFDM-THz COF** was synthesized via the reaction of benzene-1,3,5-tricarbohydrazide (THz) and 2,5-dimethoxyterephthalaldehyde (DFDM). Although the alkoxy group exists in **DFDM-THz COF**, its position is not close to the N—H group, hindering the proton transferring from N—H to the alkoxy group. This is verified by the FT-IR spectra with no change after UV irradiation for 12 h (Figure S22). These results strongly suggest that the existence of the alkoxy moiety and its position play important roles to the ESIPT process and the isomerization of acylhydrazone in COFs. In addition, we also tested the model compound of **PEG-COF-42**, which did not show any change for the FT-IR spectrum. This result suggests that the framework structure of COFs is necessary for the photoinduced isomerization (Figure S23).

As predicted, **COF-42** containing the same skeleton as **PEG-COF-42** should show a photoswitch property. UV/vis, FT-IR, XPS, and fluorescence spectra revealed results similar to those of **PEG-COF-42**. After irradiation for 12 h, it was observed the UV band of λ_{max} = 375 nm disappeared, and a new UV band (λ_{max} = 365 nm) appeared (Figure S24), indicating the isomerization from **COF-42(E)** to **COF-42(Z)**.[43] FT-IR spectra showed the characteristic peak at 1535 cm^{-1} ascribed to the bending vibration of the N—H group of acylhydrazone having gradually disappeared as irradiation time was extended (Figure S25). The intensity of the characteristic emission peak decreased after UV irradiation (Figure S26), and the intensity of C═O (531.2 eV) in XPS O 1s spectra decreased as well (Figure S27). These results strongly suggest that **COF-42** has demonstrated an acylhydrazone photoswitch behavior under UV irradiation. Based on the above results and analyses, we can conclude that the configurational change of acylhydrazone (i.e., E ↔ Z isomerization) in **COF-42** and **PEG-COF-42** is accompanied by an ESIPT process intramolecularly transferring hydrogen from hydrogen donors of N—H to hydrogen acceptors of alkoxy moieties (Figure 6a). During light irradiation, the hexagonal channels of COFs can perform a volume shrink that induced the photomechanical behavior (Figure 6b,c). Surprisingly, **COF-42** membranes exhibited no photomechanical motion under UV irradiation even after 12 h (Figure S28). As aforementioned, because the **COF-42** membrane was formed by loosely packed particles (Figure S5), it possessed a very weak mechanical property and was easily broken under mechanical force. Therefore, due to the lack of a strong connection among particles in **COF-42**, the mechanical motion of independent particles cannot be aggregated together to perform macroscopic motions. These results indicate that the PEG linkage in **PEG-COF-42** plays a key role to the stimuli-responsive behavior of **PEG-COF-42**. PEG linkers can cross-link COF particles to form integral membrane structures and transfer the microscopic motions of COFs or PEG moieties to macroscopic motions. Moreover, PEG linkers can function as "springs" that can help to stabilize the Z isomer and meanwhile promote the reversibility of the volume change of COFs.

■ CONCLUSION

In conclusion, we created a new approach to introduce PEG linkers to the **COF-42** platform and successfully fabricated a new type of uniform, highly flexible, freestanding pure COF membranes (**PEG-COF-42**). These membranes exhibited outstanding mechanical properties, comparable to some commercial or classic polymeric membranes (e.g., **PIM-1** and PVDF). Notably, **PEG-COF-42** membranes possessed a fast mechanical response (e.g., bending) to UV light, and the bending process is reversible upon thermal treatment or blue light irradiation. Various techniques such as in situ FT-IR, Raman, and XPS spectra were applied to unveil the mechanism behind the photoresponsive behavior. All results and analyses point out an unprecedented mechanism for the photoresponsive performance: configurational change of acylhydrazone (i.e., E ↔ Z isomerization) accompanied by an ESIPT process intramolecularly transferring hydrogen from the hydrogen donor groups of N—H in acylhydrazone to hydrogen acceptor groups (i.e., oxygen in PEG). Attributed to the 2D COF layer stacking structure, the Z isomer formed after UV irradiation can be stabilized through noncovalent interactions such as $\pi\cdots\pi$ stacking interaction, and the cross-linking effect of PEG linkers. In addition, we found that **PEG-COF-42** membranes can inherit the property of PEG-based building blocks, i.e., vapor-responsive behavior. By contrast, the pure **COF-42** membrane without PEG moieties exhibited no response to UV light or vapor. These interesting results further validate the crucial role of PEG in **PEG-COF-42**: (i) cross-linking COF particles to form integral membrane structures; (ii) serving as proton acceptors during the ESIPT process; (iii) transferring the microscopic motions of COFs or PEG moieties to macroscopic motions; and (iv) functioning as "springs" to stabilize the Z isomer and promoting the reversibility of volume change of the COF structure. This study not only points out a new application direction (i.e.,

https://dx.doi.org/10.1021/acscentsci.0c00260
ACS Cent. Sci. XXXX, XXX, XXX−XXX

photoresponsive artificial muscle) for COF materials but also unveiled a new mechanism for the photoswitch performance of acylhydrazone-based materials.

EXPERIMENTAL SECTION

Syntheses of PEG-COF-42. PEG-COF-42 membranes were synthesized in a 25 mL glass beaker. First, 0.0375 mmol of DTH-dimer-*x* was dissolved in the mixture solvent of 1.0 mL of H_2O and 1.0 mL of dioxane was added as a bottom layer in the beaker. TB (0.025 mmol, 4.0 mg) and 525 μL of CH_3COOH were dissolved into 3.0 mL of mesitylene and then slowly added on the top of the hydrazine layer. The system was kept at room temperature for 48 h without disturbance. Membranes were formed at the interface and then transferred into CH_3OH. The membranes were washed with CH_3OH in a Soxhlet extractor for 48 h and then dried by a supercritical carbon dioxide dryer.

Safety Statement. No unexpected or unusually high safety hazards were encountered.

ASSOCIATED CONTENT

Supporting Information

The Supporting Information is available free of charge at https://pubs.acs.org/doi/10.1021/acscentsci.0c00260.

Detailed experimental procedures, materials, FT-IR, PXRD, and SEM (PDF)

AUTHOR INFORMATION

Corresponding Author

Zhenjie Zhang − *State Key Laboratory of Medicinal Chemical Biology, College of Chemistry, Renewable Energy Conversion and Storage Center, and Key Laboratory of Advanced Energy Materials Chemistry, Ministry of Education, Nankai University, Tianjin 300071, China;* orcid.org/0000-0003-2053-3771; Email: zhangzhenjie@nankai.edu.cn

Authors

Xiuxiu Guo − *State Key Laboratory of Medicinal Chemical Biology, College of Chemistry, Nankai University, Tianjin 300071, China*

Tianhui Mao − *State Key Laboratory of Medicinal Chemical Biology, College of Chemistry, Nankai University, Tianjin 300071, China*

Zhifang Wang − *State Key Laboratory of Medicinal Chemical Biology, College of Chemistry, Renewable Energy Conversion and Storage Center, and Key Laboratory of Advanced Energy Materials Chemistry, Ministry of Education, Nankai University, Tianjin 300071, China*

Peng Cheng − *State Key Laboratory of Medicinal Chemical Biology, College of Chemistry, Renewable Energy Conversion and Storage Center, and Key Laboratory of Advanced Energy Materials Chemistry, Ministry of Education, Nankai University, Tianjin 300071, China;* orcid.org/0000-0003-0396-1846

Yao Chen − *State Key Laboratory of Medicinal Chemical Biology, College of Chemistry, Nankai University, Tianjin 300071, China;* orcid.org/0000-0002-3465-7380

Shengqian Ma − *Department of Chemistry, University of South Florida, Tampa, Florida 33620, United States;* orcid.org/0000-0002-1897-7069

Complete contact information is available at: https://pubs.acs.org/10.1021/acscentsci.0c00260

Author Contributions

The manuscript was written through contributions of all authors. All authors have given approval to the final version of the manuscript.

Notes

The authors declare no competing financial interest.

ACKNOWLEDGMENTS

The authors acknowledge the National Natural Science Foundation of China (21971126) and 111 Project (B12015).

REFERENCES

(1) Lv, J.-A.; Liu, Y.; Wei, J.; Chen, E.; Qin, L.; Yu, Y. Photocontrol of Fluid Slugs in Liquid Crystal Polymer Microactuators. *Nature* **2016**, *537*, 179−184.

(2) Cao, J.; Zhou, C.; Su, G.; Zhang, X.; Zhou, T.; Zhou, Z.; Yang, Y. Arbitrarily 3D Configurable Hygroscopic Robots with a Covalent-Noncovalent Interpenetrating Network and Self-Healing Ability. *Adv. Mater.* **2019**, *31*, 1900042.

(3) Jiang, Z.-C.; Xiao, Y.-Y.; Tong, X.; Zhao, Y. Selective Decrosslinking in Liquid Crystal Polymer Actuators for Optical Reconfiguration of Origami and Light-Fueled Locomotion. *Angew. Chem., Int. Ed.* **2019**, *58*, 5332−5337.

(4) Ghosh, S.; Mishra, M. K.; Ganguly, S.; Desiraju, G. R. Dual Stress and Thermally Driven Mechanical Properties of the Same Organic Crystal: 2,6-Dichlorobenzylidene-4-fluoro-3-nitroaniline. *J. Am. Chem. Soc.* **2015**, *137*, 9912−9921.

(5) Yu, Q.; Aguila, B.; Gao, J.; Xu, P.; Chen, Q.; Yan, J.; Xing, D.; Chen, Y.; Cheng, P.; Zhang, Z.; Ma, S. Photomechanical Organic Crystals as Smart Materials for Advanced Applications. *Chem. - Eur. J.* **2019**, *25*, 5611−5622.

(6) Han, D.-D.; Zhang, Y.-L.; Ma, J.-N.; Liu, Y.-Q.; Han, B.; Sun, H.-B. Light-Mediated Manufacture and Manipulation of Actuators. *Adv. Mater.* **2016**, *28*, 8328−8343.

(7) Duan, Y.; Semin, S.; Tinnemans, P.; Cuppen, H.; Xu, J.; Rasing, T. Robust thermoelastic microactuator based on an organic molecular crystal. *Nat. Commun.* **2019**, *10*, 4573.

(8) Xiong, X.; del Campo, A.; Cui, J. Photoresponsive Polymers. *Smart Polymers and their Applications* **2019**, 87−153.

(9) Yang, M.; Yuan, Z.; Liu, J.; Fang, Z.; Fang, L.; Yu, D.; Li, Q. Photoresponsive Actuators Built from Carbon-Based Soft Materials. *Adv. Opt. Mater.* **2019**, *7*, 1900069.

(10) Ma, S.; Li, X.; Huang, S.; Hu, J.; Yu, H. A Light-Activated Polymer Composite Enables On-Demand Photocontrolled Motion: Transportation at the Liquid/Air Interface. *Angew. Chem., Int. Ed.* **2019**, *58*, 2655−2659.

(11) Priimagi, A.; Shimamura, A.; Kondo, M.; Hiraoka, T.; Kubo, S.; Mamiya, J.-I.; Kinoshita, M.; Ikeda, T.; Shishido, A. Location of the Azobenzene Moieties within the Cross-Linked Liquid-Crystalline Polymers Can Dictate the Direction of Photoinduced Bending. *ACS Macro Lett.* **2012**, *1*, 96−99.

(12) Takashima, Y.; Hatanaka, S.; Otsubo, M.; Nakahata, M.; Kakuta, T.; Hashidzume, A.; Yamaguchi, H.; Harada, A. Expansion-Contraction of Photoresponsive Artificial Muscle Regulated by Host-Guest Interactions. *Nat. Commun.* **2012**, *3*, 1−8.

(13) Montero de Espinosa, L.; Meesorn, W.; Moatsou, D.; Weder, C. Bioinspired Polymer Systems with Stimuli-Responsive Mechanical Properties. *Chem. Rev.* **2017**, *117*, 12851−12892.

(14) Yu, H.-T.; Tang, J.-W.; Feng, Y.-Y.; Feng, W. Structural Design and Application of Azo-based Supramolecular Polymer Systems. *Chin. J. Polym. Sci.* **2019**, *37*, 1183−1199.

(15) Luo, W.; Feng, Y.; Cao, C.; Li, M.; Liu, E.; Li, S.; Qin, C.; Hu, W.; Feng, W. A High Energy Density Azobenzene/Graphene Hybrid: A Nano-Templated Platform for Solar Thermal Storage. *J. Mater. Chem. A* **2015**, *3*, 11787−11795.

(16) Si, Q.; Feng, Y.; Yang, W.; Fu, L.; Yan, Q.; Dong, L.; Long, P.; Feng, W. Controllable and Stable Deformation of a Self-Healing

Photo-Responsive Supramolecular Assembly for an Optically Actuated Manipulator Arm. *ACS Appl. Mater. Interfaces* **2018**, *10*, 29909−29917.
(17) Kim, T.; Zhu, L.; Mueller, L. J.; Bardeen, C. J. Mechanism of Photoinduced Bending and Twisting in Crystalline Microneedles and Microribbons Composed of 9-Methylanthracene. *J. Am. Chem. Soc.* **2014**, *136*, 6617−6625.
(18) Abendroth, J. M.; Bushuyev, O. S.; Weiss, P. S.; Barrett, C. J. Controlling Motion at the Nanoscale: Rise of the Molecular Machines. *ACS Nano* **2015**, *9*, 7746−7768.
(19) Zhu, L.; Al-Kaysi, R. O.; Bardeen, C. J. Photoinduced Ratchet-Like Rotational Motion of Branched Molecular Crystals. *Angew. Chem., Int. Ed.* **2016**, *55*, 7073−7076.
(20) Yu, Q.; Yang, X.; Chen, Y.; Yu, K.; Gao, J.; Liu, Z.; Cheng, P.; Zhang, Z.; Aguila, B.; Ma, S. Fabrication of Light-Triggered Soft Artificial Muscles via a Mixed-Matrix Membrane Strategy. *Angew. Chem., Int. Ed.* **2018**, *57*, 10192−10196.
(21) Morimoto, M.; Irie, M. A Diarylethene Cocrystal that Converts Light into Mechanical Work. *J. Am. Chem. Soc.* **2010**, *132*, 14172−14178.
(22) Kim, T.; Zhu, L.; Al-Kaysi, R. O.; Bardeen, C. J. Organic photomechanical materials. *ChemPhysChem* **2014**, *15*, 400−414.
(23) Naumov, P.; Chizhik, S.; Panda, M. K.; Nath, N. K.; Boldyreva, E. Mechanically Responsive Molecular Crystals. *Chem. Rev.* **2015**, *115*, 12440−12490.
(24) Côté, A. P.; Benin, A. I.; Ockwig, N. W.; O'Keeffe, M.; Matzger, A. J.; Yaghi, O. M. Porous, Crystalline, Covalent Organic Frameworks. *Science* **2005**, *310*, 1166−1170.
(25) Chen, X.; Geng, K.; Liu, R.; Tan, K. T.; Gong, Y.; Li, Z.; Tao, S.; Jiang, Q.; Jiang, D. Covalent Organic Frameworks: Chemical Approaches to Designer Structures and Built-In Functions. *Angew. Chem., Int. Ed.* **2020**, *59*, 5050−5091.
(26) Guan, X.; Chen, F.; Fang, Q.; Qiu, S. Design and Applications of Three Dimensional Covalent Organic Frameworks. *Chem. Soc. Rev.* **2020**, *49*, 1357−1384.
(27) Zhang, J.; Han, X.; Wu, X.; Liu, Y.; Cui, Y. Multivariate Chiral Covalent Organic Frameworks with Controlled Crystallinity and Stability for Asymmetric Catalysis. *J. Am. Chem. Soc.* **2017**, *139*, 8277−8285.
(28) Fan, H.; Mundstock, A.; Feldhoff, A.; Knebel, A.; Gu, J.; Meng, H.; Caro, J. Covalent Organic Framework-Covalent Organic Framework Bilayer Membranes for Highly Selective Gas Separation. *J. Am. Chem. Soc.* **2018**, *140*, 10094−10098.
(29) Shao, P.; Li, J.; Chen, F.; Ma, L.; Li, Q.; Zhang, M.; Zhou, J.; Yin, A.; Feng, X.; Wang, B. Flexible Films of Covalent Organic Frameworks with Ultralow Dielectric Constants under High Humidity. *Angew. Chem., Int. Ed.* **2018**, *57*, 16501−16505.
(30) Evans, A. M.; Parent, L. R.; Flanders, N. C.; Bisbey, R. P.; Vitaku, E.; Kirschner, M. S.; Schaller, R. D.; Chen, L. X.; Gianneschi, N. C.; Dichtel, W. R. Seeded growth of single-crystal two-dimensional covalent organic frameworks. *Science* **2018**, *361*, 52−57.
(31) Dey, K.; Pal, M.; Rout, K. C.; Kunjattu H, S.; Das, A.; Mukherjee, R.; Kharul, U. K.; Banerjee, R. Selective Molecular Separation by Interfacially Crystallized Covalent Organic Framework Thin Films. *J. Am. Chem. Soc.* **2017**, *139*, 13083−13091.
(32) Zeng, Y.; Zou, R.; Luo, Z.; Zhang, H.; Yao, X.; Ma, X.; Zou, R.; Zhao, Y. Covalent Organic Frameworks Formed with Two Types of Covalent Bonds Based on Orthogonal Reactions. *J. Am. Chem. Soc.* **2015**, *137*, 1020−1023.
(33) Vyas, V. S.; Haase, F.; Stegbauer, L.; Savasci, G.; Podjaski, F.; Ochsenfeld, C.; Lotsch, B. V. A Tunable Azine Aovalent Organic Framework Platform for Visible Light-induced Hydrogen Generation. *Nat. Commun.* **2015**, *6*, 8508.
(34) Zhang, S.; Cheng, G.; Guo, L.; Wang, N.; Tan, B.; Jin, S. Strong-Base-Assisted Synthesis of a Crystalline Covalent Triazine Framework with High Hydrophilicity via Benzylamine Monomer for Photocatalytic Water Splitting. *Angew. Chem.* **2020**, *132*, 6063−6070.
(35) Hu, Y.; Dunlap, N.; Wan, S.; Lu, S.; Huang, S.; Sellinger, I.; Ortiz, M.; Jin, Y.; Lee, S.-h.; Zhang, W. Crystalline Lithium Imidazolate Covalent Organic Frameworks with High Li-ion Conductivity. *J. Am. Chem. Soc.* **2019**, *141*, 7518−7525.
(36) Zhang, L.; Wang, S.; Zhou, Y.; Wang, C.; Zhang, X.-Z.; Deng, H. Covalent Organic Frameworks as Favorable Constructs for Photodynamic Therapy. *Angew. Chem.* **2019**, *131*, 14351−14356.
(37) Sun, T.; Wei, L.; Chen, Y.; Ma, Y.; Zhang, Y.-B. Atomic-Level Characterization of Dynamics of a 3D Covalent Organic Framework by Cryo-Electron Diffraction Tomography. *J. Am. Chem. Soc.* **2019**, *141*, 10962−10966.
(38) Park, S.; Liao, Z.; Ibarlucea, B.; Qi, H.; Lin, H.-H.; Becker, D.; Melidonie, J.; Zhang, T.; Sahabudeen, H.; Baraban, L.; Baek, C.-K.; Zheng, Z.; Zschech, E.; Fery, A.; Heine, T.; Kaiser, U.; Cuniberti, G.; Dong, R.; Feng, X. Two-Dimensional Boronate Ester Covalent Organic Framework Thin Films with Large Single Crystalline Domains for Neuromorphic Memory Device. *Angew. Chem.* **2020**, in press. DOI: 10.1002/ange.201916595
(39) Ascherl, L.; Sick, T.; Margraf, J. T.; Lapidus, S. H.; Calik, M.; Hettstedt, C.; Karaghiosoff, K.; Döblinger, M.; Clark, T.; Chapman, K. W.; Auras, F.; Bein, T. Molecular docking sites designed for the generation of highly crystalline covalent organic frameworks. *Nat. Chem.* **2016**, *8*, 310−316.
(40) Wang, Y.; Liu, Y.; Li, H.; Guan, X.; Xue, M.; Yan, Y.; Valtchev, V.; Qiu, S.; Fang, Q. Three-Dimensional Mesoporous Covalent Organic Frameworks through Steric Hindrance Engineering. *J. Am. Chem. Soc.* **2020**, *142*, 3736−3741.
(41) Das, G.; Prakasam, T.; Addicoat, M. A.; Sharma, S. K.; Ravaux, F.; Mathew, R.; Baias, M.; Jagannathan, R.; Olson, M. A.; Trabolsi, A. Azobenzene-Equipped Covalent Organic Framework: Light-Operated Reservoir. *J. Am. Chem. Soc.* **2019**, *141*, 19078−19087.
(42) Su, X.; Aprahamian, I. Hydrazone-Based Switches, Metallo-Assemblies and Sensors. *Chem. Soc. Rev.* **2014**, *43*, 1963−1981.
(43) van Dijken, D. J.; Kovaříček, P.; Ihrig, S. P.; Hecht, S. Acylhydrazones as Widely Tunable Photoswitches. *J. Am. Chem. Soc.* **2015**, *137*, 14982−14991.
(44) Gupta, P.; Panda, T.; Allu, S.; Borah, S.; Baishya, A.; Gunnam, A.; Nangia, A.; Naumov, P.; Nath, N. K. Crystalline Acylhydrazone Photoswitches with Multiple Mechanical Responses. *Cryst. Growth Des.* **2019**, *19*, 3039−3044.
(45) Cvrtila, I.; Fanlo-Virgós, H.; Schaeffer, G.; Santiago, G. M.; Otto, S. Redox Control over Acyl Hydrazone Photoswitches. *J. Am. Chem. Soc.* **2017**, *139*, 12459−12465.
(46) Uribe-Romo, F. J.; Doonan, C. J.; Furukawa, H.; Oisaki, K.; Yaghi, O. M. Crystalline Covalent Organic Frameworks with Hydrazone Linkages. *J. Am. Chem. Soc.* **2011**, *133*, 11478−11481.
(47) Li, X.; Qiao, J.; Chee, S. W.; Xu, H.-S.; Zhao, X.; Choi, H. S.; Yu, W.; Quek, S. Y.; Mirsaidov, U.; Loh, K. P. Rapid, Scalable Construction of Highly Crystalline Acylhydrazone Two-dimensional Covalent Organic Frameworks via Dipole-Induced Antiparallel Stacking. *J. Am. Chem. Soc.* **2020**, *142*, 4932−4943.
(48) Ding, S.-Y.; Cui, X.-H.; Feng, J.; Lu, G.; Wang, W. Facile Synthesis of -C═N- Linked Covalent Organic Frameworks under Ambient Conditions. *Chem. Commun.* **2017**, *53*, 11956−11959.
(49) Wang, Z.; Yu, Q.; Huang, Y.; An, H.; Zhao, Y.; Feng, Y.; Li, X.; Shi, X.; Liang, J.; Pan, F.; Cheng, P.; Chen, Y.; Ma, S.; Zhang, Z. PolyCOFs: A New Class of Freestanding Responsive Covalent Organic Framework Membranes with High Mechanical Performance. *ACS Cent. Sci.* **2019**, *5*, 1352−1359.
(50) Saleh, M. I.; Kusrini, E.; Saad, B.; Fun, H.-K.; Yamin, B. M. Coordination of Trivalent Lanthanum with Polyethylene Glycol in the Presence of Picrate Anion: Spectroscopic and X-ray Structural Studies. *J. Alloys Compd.* **2009**, *474*, 428−440.
(51) Koshima, H.; Ojima, N.; Uchimoto, H. Mechanical motion of azobenzene crystals upon photoirradiation. *J. Am. Chem. Soc.* **2009**, *131*, 6890−6891.
(52) Li, X.; Gao, Q.; Wang, J.; Chen, Y.; Chen, Z. H.; Xu, H. S.; Tang, W.; Leng, K.; Ning, G. H.; Wu, J.; Xu, Q. H.; Quek, S. Y.; Lu, Y.; Loh, K. P. Tuneable Near White-Emissive Two-Dimensional Covalent Organic Frameworks. *Nat. Commun.* **2018**, *9*, 2335.

https://dx.doi.org/10.1021/acscentsci.0c00260
ACS Cent. Sci. XXXX, XXX, XXX−XXX

(53) Coman, A. G.; Paun, A.; Popescu, C. C.; Hădade, N. D.; Anghel, C. C.; Mădălan, A. M.; Ionită, P.; Matache, M. Conformation-Induced Light Emission Switching of N-Acylhydrazone Systems. *New J. Chem.* **2018**, *42*, 14111−14119.
(54) Lehn, J.-M. Conjecture: Imines as Unidirectional Photodriven Molecular Motors-Motional and Constitutional Dynamic Device. *Chem. - Eur. J.* **2006**, *12*, 5910−5915.

https://dx.doi.org/10.1021/acscentsci.0c00260
ACS Cent. Sci. XXXX, XXX, XXX−XXX